JACS
JOURNAL OF THE AMERICAN CHEMICAL SOCIETY
Article
pubs.acs.org/JACS

Efficient Singlet Fission Discovered in a Disordered Acene Film

Sean T. Roberts, R. Eric McAnally, Joseph N. Mastron, David H. Webber, Matthew T. Whited,‡ Richard L. Brutchey, Mark E. Thompson,* and Stephen E. Bradforth*

Department of Chemistry and the Center for Energy Nanoscience, University of Southern California, Los Angeles, California 90089-0482, United States

Supporting Information

ABSTRACT: Singlet exciton fission is a process that occurs in select organic semiconductors and entails the splitting of a singlet excited state into two lower triplet excitons located on adjacent chromophores. Research examining this phenomenon has recently seen a renaissance due to the potential to exploit singlet fission within the context of organic photovoltaics to prepare devices with the ability to circumvent the Shockley–Queisser limit. To date, high singlet fission yields have only been reported for crystalline or polycrystalline materials, suggesting that molecular disorder inhibits singlet fission. Here, we report the results of ultrafast transient absorption and time-resolved emission experiments performed on 5,12-diphenyl tetracene (DPT). Unlike tetracene, which tends to form polycrystalline films when vapor deposited, DPT's pendant phenyl groups frustrate crystal growth, yielding amorphous films. Despite the high level of disorder in these films, we find that DPT exhibits a surprisingly high singlet fission yield, with 1.22 triplets being created per excited singlet. This triplet production occurs over two principal time scales, with ~50% of the triplets appearing within 1 ps after photoexcitation followed by a slower phase of triplet growth over a few hundred picoseconds. To fit these kinetics, we have developed a model that assumes that due to molecular disorder, only a subset of DPT dimer pairs adopt configurations that promote fission. Singlet excitons directly excited at these sites can undergo fission rapidly, while singlet excitons created elsewhere in the film must diffuse to these sites to fission.

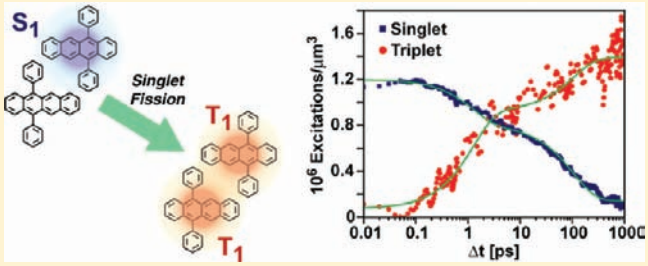

I. INTRODUCTION

As was first outlined by Shockley and Queisser in 1961,[1] one of the predominant loss mechanisms that limits the performance of photovoltaic cells is the rapid dissipation of the excess energy of supra-band gap photons as heat, leading to a maximum theoretical efficiency of 31% for a single-junction device. One strategy that has the potential to circumvent this energy loss is to use high energy photons to excite more than a single electron–hole pair. This process, referred to as multiple exciton generation (MEG), has been found to occur in inorganic colloidal nanoparticles.[2] However, studies investigating MEG have reported onset thresholds in excess of the theoretical prediction of 2 times the nanoparticle band gap,[3,4] eliminating much of the potential improvement in power conversion efficiency that can result from MEG.[5]

Singlet fission (SF) is a phenomenon observed in molecular systems that, like MEG, has the potential to generate more than one electron–hole pair from a single photoexcitation. SF is a spin-allowed process wherein a singlet exciton divides its energy to form two triplet excited states located on neighboring molecules.[6] First observed in anthracene crystals in 1965,[7] SF has subsequently been found to occur in numerous systems, including large polyacenes (tetracene, pentacene),[8−12] diacetylene and thiophene polymers,[13−15] and carotenoids.[16] Organic photovoltaics (OPVs) that utilize a SF material to absorb high energy green photons and a complementary red absorber to capture infrared photons are predicted to have limiting power conversion efficiencies near 45%,[5] roughly a 40% increase over the Shockley–Queisser limit.

As a spin-allowed process, SF can be exceptionally fast, occurring over femtosecond to picosecond time scales. Ultrafast transient absorption experiments performed on tetracene films,[11,17−19] where SF is thermally activated ($2E(T_1) - E(S_1) = 0.19-0.24$ eV),[20−22] have found that the rate of triplet formation falls in the range of 40–90 ps. In pentacene thin films, where SF is exergonic ($2E(T_1) - E(S_1) = -0.11$ eV),[22] the rate of triplet formation accelerates to 80 fs.[23] The rapidity with which SF occurs allows it to efficiently compete with other relaxation processes, leading to the possibility of high SF yields. Recent studies investigating SF in polycrystalline acene films,[12,18] carotenoid J-aggregates,[16] and polycrystalline thin films of the biradicaloid 1,3-diphenylisobenzofuran[24] have reported triplet generation yields over 100% (>50% SF yield), raising the prospects for the realization of SF-based commercial devices. Indeed, photodetectors utilizing thin pentacene films[25] have exhibited quantum efficiencies in excess of 100%, and SF has been found to augment the performance of a tetracene-based photovolatic.[26]

While the library of compounds that have been shown to undergo SF continues to grow,[6,27] little information is currently known regarding the reaction coordinates that control SF.

Received: January 16, 2012
Published: March 20, 2012

   dx.doi.org/10.1021/ja300504t | J. Am. Chem. Soc. 2012, 134, 6388–6400

While SF has been found to occur to a limited extent in partially disordered systems,[15,28,29] to date a common theme that characterizes systems with high SF yields is a large degree of crystallinity. Experiments that have examined SF compounds constrained to geometries that differ from their normal crystal packing arrangements tend to show reduced SF yields. For example, while polycrystalline tetracene films show high SF yields,[18] similar measurements on covalently tethered tetracene dimers display SF yields of only 2−3%.[9] Likewise, experiments comparing the behavior of pentacene single crystals and vapor deposited pentacene films found that SF is suppressed in vapor deposited films,[11] while measurements of pentacene films grown on a polymer substrate suggest that the dominant species created by photoexcitation is a singlet excimer state, with SF only occurring for 2% of the initial excitations.[28,29] Recent ab initio calculations of pentacene and tetracene crystals have suggested that lattice vibrations within a crystal may in fact act as a reaction coordinate for SF.[30,31] This is supported by femtosecond pulse-shaping experiments that demonstrate that the SF yield of polycrystalline tetracene films can be increased through the excitation of crystal phonon modes.[17]

Taken together, these results suggest that the rate of SF depends intimately on the way in which neighboring chromophores are organized, which has implications for the prospect of future SF-based OPVs. The lower production costs of OPVs as compared to existing solar technologies result in part from the ability to produce OPVs using inexpensive solution processing techniques, such as roll-to-roll printing,[32] that generally afford only limited control over the resulting film morphology. Thus, understanding how SF depends on the intermolecular arrangement of chromophores and if it is possible to retain a high SF yield in films with a high degree of molecular disorder are questions pertinent to the future production of commercial SF-based OPVs.

With these ideas in mind, we have investigated the interplay of singlet and triplet excitons within thin films of 5,12-diphenyl tetracene (DPT). The addition of two substituent phenyl groups frustrates crystal growth during the vapor deposition process, yielding DPT films that are largely amorphous. Steric effects prevent the pendant phenyl groups from conjugating to the tetracene core, ensuring that the electronic properties of DPT are only slightly altered from those of tetracene. This allows the influence of morphology on SF to be tested directly. In a prior report, we characterized the spectral signatures of DPT's lowest excited triplet state by doping DPT films with a platinum porphyrin triplet sensitizer.[33] Here, we utilize this information in conjunction with ultrafast transient absorption (TA) and time-resolved emission experiments to track the kinetics that govern SF in DPT films. Surprisingly, despite the high degree of disorder present in amorphous DPT films, the SF yield remains remarkably high, with 61% of excited singlets fissioning to two triplets. Approximately one-half of the produced triplets are generated within 1 ps, while the remaining triplet production occurs over the course of ∼100 ps. To model this behavior, we have constructed a kinetic model that treats the production of triplet excitons as a diffusion-limited process, with singlet excitons first diffusing to locations where pairs of DPT molecules adopt configurations conducive to SF. This model also accounts for effects due to both singlet exciton−exciton annihilation, and the regeneration of singlet excitons via SF's reverse reaction, triplet−triplet annihilation. Our results indicate that a high SF yield can be obtained even in a disordered molecular film with minimal coupling between neighboring chromophores, brightening the prospects for low-cost, SF-based OPVs.

II. EXPERIMENTAL METHODS

Sample Preparation. DPT was synthesized according to literature procedures,[34,35] while tetracene was obtained from Aldrich. Both materials were purified via vacuum thermal gradient sublimation (2×) prior to use. Samples consisted of either compound dissolved in either $CHCl_3$ or vapor deposited (2−3 Å/s) as a thin film on a 1/16" quartz substrate. $CHCl_3$ solution samples used in both TA and emission studies were held in a 1 cm path length quartz cell, and the solution concentration was adjusted to give a peak optical density below 0.1. Film samples used for either TA or time-resolved emission studies had an additional quartz window placed on top of the film, and the outside edges were sealed with epoxy under a N_2 atmosphere to prevent sample photooxidation. The thickness of these films was ∼100 nm, yielding an optical density of ∼0.3 at 500 nm.

Film Characterization. Absorption spectra were obtained using a Cary 50 UV−vis spectrometer in transmission geometry. Film and solution spectra were corrected for spurious signal contributions from scattered light by fitting the baseline of each spectrum to a polynomial function between 750 and 1000 nm where no sample absorption features appear. Steady-state emission spectra were measured with a Horiba FluoroMax-3 using a right angle collection geometry. To suppress line shape changes due to sample reabsorption, the thickness of sample films used for steady-state emission studies was set at 10 nm. 435 nm light was used to excite DPT film samples, while a slightly shorter wavelength of 400 nm was used for DPT dissolved in $CHCl_3$ solution. Tetracene solution and film samples were excited at 420 and 425 nm, respectively.

The morphology of sample films was studied with grazing incidence X-ray diffraction measurements (XRD), transmission electron microscopy (TEM), and selected area electron diffraction (SAED). XRD measurements were performed on a Rigaku Ultima IV diffractometer using a Cu Kα radiation source (λ = 1.54 Å). Samples were prepared for TEM and SAED by evaporating films onto a copper TEM grid faced with an ultrathin-carbon film supported on holey carbon (Ted Pella 01824). TEM images and SAED patterns were acquired on a JEOL JEM-2100 fitted with a Gatan Orius CCD digital camera, using an accelerating voltage of 200 kV. Because the films degrade over a period of a few seconds under electron bombardment, the diffraction experiments were conducted by having the CCD camera continuously refresh the image, rapidly moving the film to a fresh location, and immediately saving the resulting diffraction pattern. Numerous areas of each film were examined in this way to ensure reliability of the results.

X-ray Crystallography. Crystals of DPT were grown by sublimation in a three zone tube furnace, held at a pressure of 0.2 μTorr. The three zones were set to 250, 220, and 170 °C, with the solid DPT sample placed in the hot zone. The DPT transports down the tube, with crystals growing in the second zone. Diffraction data for DPT were collected on a Bruker SMART APEX CCD diffractometer with graphite-monochromated Mo Kα radiation (λ = 0.71073 Å). The cell parameters for the complexes were obtained from a least-squares refinement of the spots (from 60 collected frames) using the SMART program. One hemisphere of crystal data was collected up to a resolution of 0.80 Å, and the intensity data were processed using the Saint Plus program. All of the calculations for the structure determination were carried out using the SHELXTL package (Version 5.1). Hydrogen atoms were located in the difference map, and their positions were refined freely. A summary of the refinement details and the resulting factors are given in Table S1 of the Supporting Information.

Ultrafast Nonlinear Spectroscopy. Time-resolved emission data were recorded using a time-correlated single photon counting (TCSPC) system (Becker and Hickl SPC 630) operating in tandem with a 250 kHz Ti-sapphire regenerative amplifier (Coherent RegA 9050). Excitation pulses centered at 505 nm were produced using a 400 nm pumped type I optical parametric amplifier (Coherent OPA

9450). The resulting fluorescence emission was collected at a right angle to the sample, passed through a 0.125 m double monochromator (Digikröm CM112) set to transmit 535 nm light, and detected using a Hamamatsu R3809U-50 photomultiplier tube with a 20 ps instrument response time. The presented data measured for DPT films were recorded using a pump fluence of 0.5 $\mu J/cm^2$, while data for DPT dissolved in $CHCl_3$ were measured at lower fluence, 0.1 $\mu J/cm^2$. All reported data were measured for magic angle polarization.

Femtosecond TA measurements were carried out using the output of a Coherent Legend Ti:sapphire amplifier operating at a 1 kHz repetition rate. Approximately 10% of the amplifier's output was used to seed a type II Spectra Physics OPA-800C, generating excitation pulses centered at 500 nm with ~9 nm of bandwidth. White light supercontinuum probe pulses (320–950 nm) were produced by focusing a small portion of the amplifier output into a 2 mm thick CaF_2 window that was continuously rotated to both prevent photodamage and ensure the stability of the continuum probe. To minimize probe dispersion, a pair of off-axis aluminum parabolic mirrors were used to collimate the probe and focus it into the sample, while a CaF_2 lens focused the pump. Following the sample, a spectrograph (Oriel MS1271) dispersed the probe onto a 256 pixel silicon array (Hamamatsu). The time resolution of the system was found to be 200 fs based on a cross-correlation between the pump and probe in a 1 mm quartz substrate. All presented transient spectra were recorded using magic angle polarization conditions. Spectra were measured for a range of excitation fluences from 3.7 to 96 $\mu J/cm^2$, as noted in the text. Samples were slowly translated perpendicular to the path of the pump and probe by a linear stage to prevent photodamage.

III. CHARACTERIZATION OF THE STRUCTURE OF VAPOR DEPOSITED DPT FILMS

To understand the structure of vapor deposited DPT films, XRD and TEM experiments were performed on sample films, the results of which were compared to similar data measured for vapor deposited tetracene. A summary of these results appears in Figure 1. XRD data measured for tetracene films show two strong diffraction peaks at 2θ values of 7.1° and 14.5° that correspond to scattering from tetracene's 001 and 002 planes, respectively.[36] In contrast, no diffraction peaks are observed for a similarly prepared DPT film, suggesting that the film is amorphous and confirming the hypothesis that the phenyl rings of DPT frustrate crystal growth. These conclusions are further supported by TEM-SAED images measured for vapor deposited tetracene and DPT films. Images recorded for tetracene (Figure 1B) show a series of strong diffraction spots, indicating that the film is crystalline. However, images measured for DPT (Figure 1C) show no discernible diffraction peaks, confirming the conclusion that the DPT films we investigate here are indeed amorphous.

To examine how the amorphous nature of DPT films affects their optical properties with respect to tetracene, the absorption and emission properties of DPT solutions and thin films were measured and compared to those of tetracene (Figure 2). Absorption and emission spectra of tetracene dissolved in $CHCl_3$ show the presence of a strong vibrational progression related to a symmetric ring breathing mode that is a characteristic spectral feature of isolated polyacenes.[37−39] When vacuum deposited, tetracene films often contain crystalline domains[18,40,41] whose structure allows for efficient electronic coupling between neighboring tetracene molecules. This is reflected in the absorption spectrum of tetracene thin films, which shifts to lower energy and shows a splitting of tetracene's vibrational progression as a result of Davydov coupling.[42,43] Likewise, the emission spectrum of tetracene thin films is red-shifted relative to solution and shows a strong

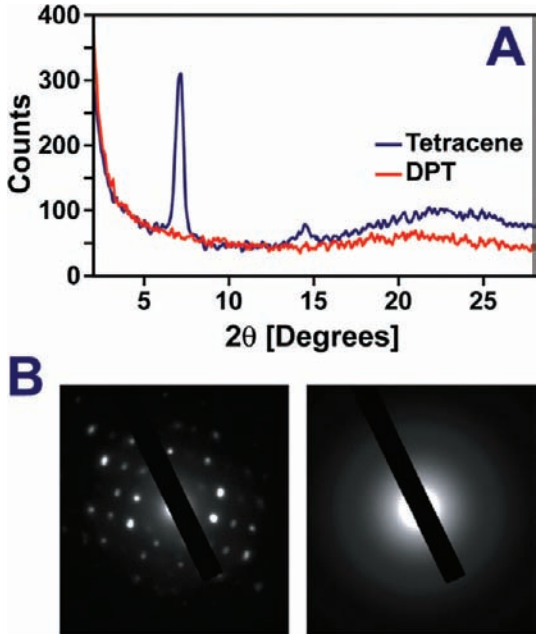

Figure 1. (A) X-ray diffraction patterns measured for vapor deposited tetracene and DPT films. Diffraction peaks corresponding to the (001) and (002) planes of tetracene are observed, while no diffraction peaks appear for DPT. The weak feature at 2θ = 21° results from the underlying glass substrate. (B) Selected area electron diffraction images measured for tetracene (left) and DPT (right) films. The lack of scattering from the DPT sample suggests that the film is largely amorphous.

enhancement of the 0–0 peak in the vibronic progression, which is a signature of the formation of delocalized J-aggregate states[44] and can be used to estimate the extent of exciton delocalization.[45] On the basis of the changes in the emission line shape between thin film and solution, Lim et al.[46] estimate that singlet excitons in tetracene crystals can be delocalized over ~10 molecules.

Spectra measured for DPT solutions show a vibronic progression similar to that observed for tetracene in $CHCl_3$, but with peak values that are shifted to lower energy by 810 cm^{-1} (19 nm) and 917 cm^{-1} (21 nm) for absorption and emission, respectively. These small shifts suggest that phenyl substitution only induces a modest perturbation to the electronic structure of DPT's tetracene core. Unlike tetracene, however, with the exception of a slight red-shift of 280 cm^{-1} (7 nm), the absorption spectrum of the vapor deposited film is nearly identical to that of DPT in solution and shows no evidence of Davydov splitting. Likewise, the emission spectrum of the DPT film is very similar to the solution spectrum, showing only a slight decrease in the ratio of the amplitudes of the first and second emission peaks in the vibronic progression. The lack of change in the absorption and emission spectra of DPT films relative to solution indicates that, unlike tetracene, the ground and first excited singlet states of DPT are relatively uncoupled, likely causing singlet excitons to only extend over single DPT molecules. Whether this lack of coupling is solely attributable to either the increased spacing between the π-systems of neighboring DPT molecules afforded by their phenyl side groups, the high degree of molecular disorder in the amorphous film, or a combination of these two effects is unclear. However, we note that the vibronic progression in the optical absorption spectra of rubrene (5,6,11,12-tetraphenyl

dx.doi.org/10.1021/ja300504t | J. Am. Chem. Soc. 2012, 134, 6388–6400

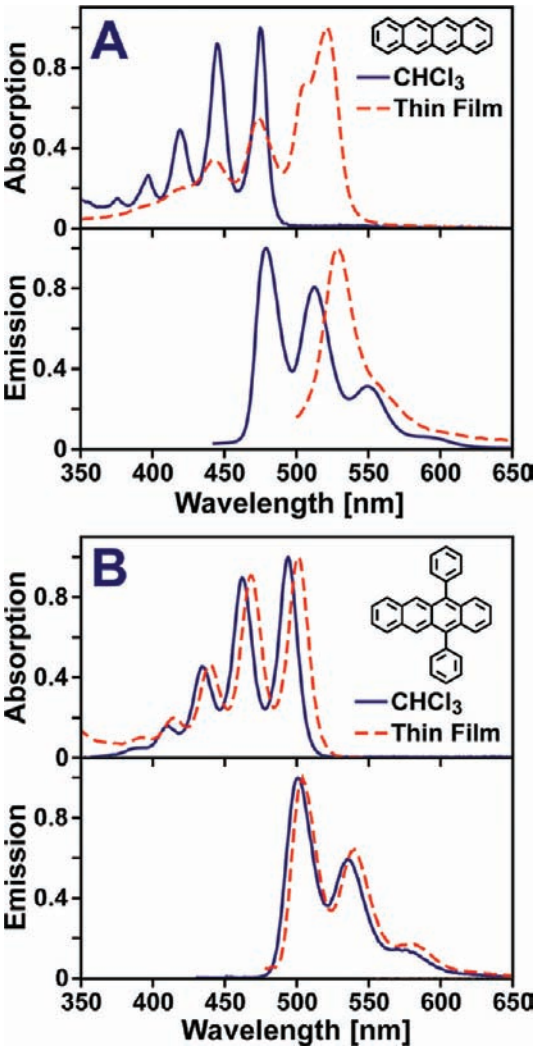

Figure 2. Optical absorption and emission spectra for tetracene (A) and DPT (B) chloroform solutions and thin films. Changes in the spectra of tetracene between solution and film arise from Davydov coupling between neighboring chromophores, while the lack of change in the spectra of DPT suggests that neighboring molecules are largely uncoupled.

tetracene) single crystals is modified from that measured in $CHCl_3$ solution due to the presence of Davydov coupling,[47] suggesting that the steric bulk provided by phenyl substitution is not sufficient to prevent coupling between neighboring molecules.

IV. TIME-RESOLVED EMISSION OF DPT FILMS AND SOLUTIONS

One of the first means by which SF was detected in acene crystals was through the observation of delayed emission in time-resolved fluorescence measurements.[7,8,20,48,49] As SF takes place, the singlet population within an acene crystal is depleted, leading to an accelerated decay of the crystal's emission relative to that measured for the isolated acene chromophore. However, if the energy of the two triplet excitons created via SF is close to that of the singlet state from which they are generated, the two triplet excitons can recombine over long time scales to regenerate a singlet exciton, resulting in emission that can persist for orders of magnitude longer than the emission lifetime of the isolated acene.

As an initial test of DPT's ability to undergo SF in vapor deposited films, we utilized TCSPC measurements to determine if these films display rapid quenching followed by delayed fluorescence. Figure 3A compares the emission

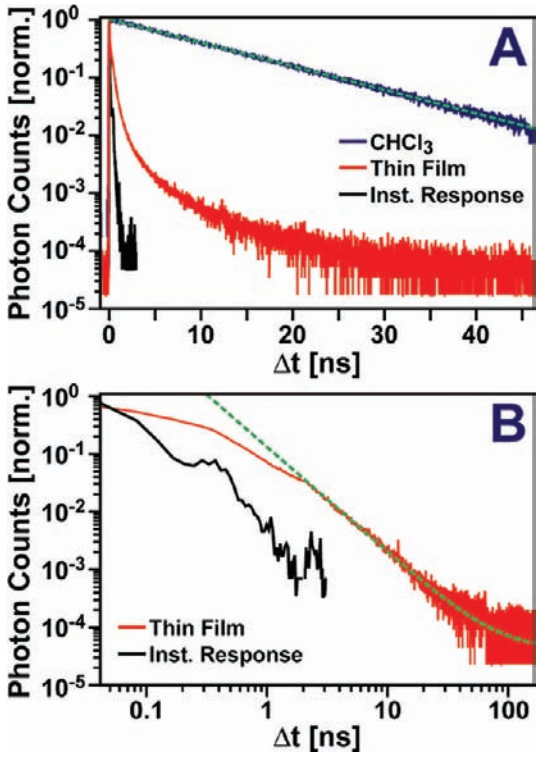

Figure 3. (A) TCSPC measurements of DPT in $CHCl_3$ (blue), a vapor deposited DPT film (red), and the TCSPC system's instrument response function (black). The emission decay measured in $CHCl_3$ fits well to a single exponential decay of 11 ns (green dashed), while the thin film emission is highly nonexponential. (B) Emission decay measured for a DPT film plotted on a log–log scale to highlight the long-lived emission tail. The green dashed line represents a $t^{-1.8}$ power law fit plus offset.

behavior of DPT in solution and vapor deposited films. DPT molecules dissolved in $CHCl_3$ exhibit a single exponential decay with an 11 ns time constant. This value is slightly faster than that previously measured for DPT in benzene, 15.2 ns,[50] and may in part reflect that the $CHCl_3$ solution was not rigorously purged of oxygen. In sharp contrast, the emission measured for vapor deposited DPT films is greatly accelerated and highly nonexponential, with 25% of the initial decay occurring within the instrument's time resolution (20 ps) and 99% of the total decay occurring within 3 ns. Despite this fast initial decay, a long-lived tail that persists for longer than 150 ns is observed in the film's emission trace (Figure 3B). The fact that this tail persists for an order of magnitude longer than the emission lifetime of DPT in solution shows that delayed fluorescence is indeed observed from DPT films. This tail can be fit well by a power law decay with an exponent of −1.8 plus a small offset. A recent study of crystalline rubrene and tetracene films has shown that over time scales longer than 300 ns, emission from the film decays as t^{-2},[51] which was rationalized using a model that assumed that the emission resulted from the regeneration of singlet excitons via triplet–triplet annihilation following SF. Given that the t^{-2} power law decay is close to the $t^{-1.8}$ decay we observe for DPT films, this suggests that the long-lived

dx.doi.org/10.1021/ja300504t | J. Am. Chem. Soc. 2012, 134, 6388–6400

emission tail is consistent with the occurrence of SF following photoexcitation.

V. TRANSIENT ABSORPTION SPECTRA OF AMORPHOUS DPT FILMS

While the rapid initial fluorescence decay in DPT films followed by long-lived emission is suggestive of SF,[7,8,18,20,48,49,51] the measurement of delayed fluorescence alone is not sufficient to confirm the presence of SF because rapid quenching followed by delayed emission may also result from the presence of fluorescent impurities. Thus, to better understand the fate of photogenerated singlet excitons in DPT films, TA experiments were used to characterize the excited-state kinetics of DPT over femtosecond time scales. Figure 4A plots TA spectra measured for DPT dissolved in $CHCl_3$. Exciting DPT at 500 nm leads to the population of its lowest excited singlet state and is reflected by the appearance of photobleach peaks at 460 and 498 nm that match the vibronic progression of DPT's ground-state absorption spectrum as well as a third photobleach feature at 540 nm due to stimulated emission from DPT's S_1 state. The most prominent feature in the transient spectrum is the strong induced absorption band at 416 nm that immediately appears following photoexcitation, and, consequently, we assign to a $S_1 \rightarrow S_n$ transition. Over the course of 1 ns, the transient spectrum exhibits no spectral changes other than a slight decay of its amplitude consistent with the 11 ns S_1 lifetime measured in TCSPC experiments. This lack of spectral evolution indicates that excited DPT molecules remain in the S_1 state during this time window.

Transient spectra measured for a vapor deposited DPT film exhibit qualitatively different behavior (Figure 4B). Initially following photoexcitation, the transient spectrum resembles that measured for DPT in $CHCl_3$. However, over the course of ~100 ps, the strong $S_1 \rightarrow S_n$ transition peak at 421 nm[52] decays, indicating the transfer of population out of DPT's S_1 state. Concurrent with this change, the growth of a new induced absorption band can be seen between 470 and 520 nm. The lowest lying triplet excited state of tetracene, as well as that of many of its derivatives, is known to absorb strongly in the range of 400–500 nm.[18,50,53,54] For tetracene and pentacene, the transition dipole of this band lies along the long axis of the molecule.[6,55] This makes the band difficult to observe in TA studies of polycrystalline films of these materials because crystallites prefer to form with their long axes aligned at a small angle with respect to the film's surface normal,[56,57] leading to minimal overlap between the electric field of the probe and the triplet transition dipole.[18,28,29,58] However, given the amorphous nature of the DPT films investigated here, the appearance of an induced absorption band between 400 and 500 nm strongly suggests the production of triplet excitons.

To determine if this new band corresponds to DPT's T_1 state, in Figure 4C we compare the transient spectrum of vapor deposited DPT at Δt = 750 ps to that previously measured for DPT triplets in experiments that utilized a triplet sensitizer, platinum tetraphenylbenzoporphyrin (PtTPBP), doped into DPT films to preferentially populate DPT's T_1 state.[33] This latter spectrum has been corrected for residual contributions from PtTPBP, yielding a line shape that signals the population of DPT's T_1 state.[59] The absorption profile of the transient spectrum of vapor deposited DPT compares favorably with that measured for DPT triplets. Both spectra peak near 490 nm and have similar linewidths, suggesting that DPT triplet excitons are produced following photoexcitation of the vapor deposited film.

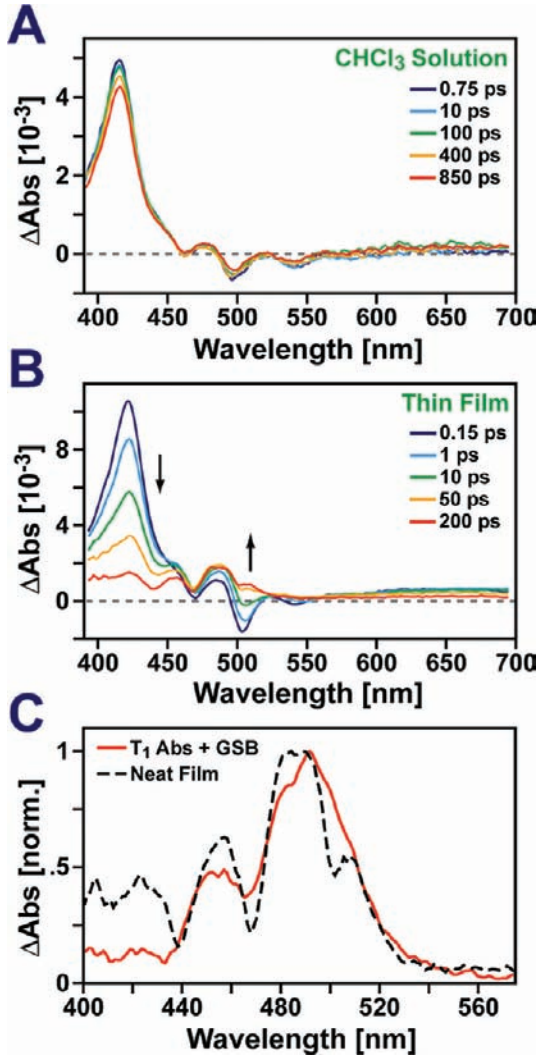

Figure 4. (A) TA spectra of DPT dissolved in $CHCl_3$ following photoexcitation at 500 nm. The strong induced absorption band at 416 nm corresponds to a $S_1 \rightarrow S_n$ transition that serves as a marker-mode for the S_1 state. (B) TA spectra of a vapor deposited DPT film measured using an excitation fluence of 31 $\mu J/cm^2$. Following photoexcitation, depopulation of the S_1 state occurs over the course of ~100 ps concomitant with the rise of a new absorption feature at ~510 nm. (C) Comparison of the TA spectrum measured for vapor deposited DPT at Δt = 750 ps (black dashed) with the transient line shape expected for the population of DPT triplet excitons (red). This latter spectrum contains equally weighted contributions from DPT T_1 excited-state absorption and ground-state bleaching (GSB). The similarity of these two spectra suggests the population of triplet excitons.

From our TCSPC experiments, we expect ~10% of the initial excited singlet population to be present in the film at a delay of 750 ps. This largely accounts for the differences between the two plotted lineshapes, notably the residual $S_1 \rightarrow S_n$ induced absorption at 421 nm and larger ground-state bleach of the neat film transient spectrum relative to the expected triplet line shape. The subnanosecond appearance of triplet excitons in vapor deposited DPT films is much faster than would be expected if triplets were produced via intersystem crossing ($1/k_{ISC}$ = 89 ns).[50] This, taken together with the observation of delayed fluorescence in TCPSC experiments, confirms that amorphous DPT films undergo SF.

dx.doi.org/10.1021/ja300504t | J. Am. Chem. Soc. 2012, 134, 6388–6400

Although bands that can be assigned to singlet and triplet excitons appear in the TA spectra of vapor deposited films, neither the decay of the S_1 induced absorption nor the rise of the T_1 absorption between 400 and 500 nm can be well fit by a single exponential function. While complicated time-dependent changes at a given wavelength partially result from overlap between singlet and triplet absorption features, other studies that have examined SF in polyacene films have noted that when singlet excitons are prepared at high density, singlet−singlet annihilation (SSA) can lead to nonexponential kinetics.[18,29,49,60,61] A recent study of tetracene films has shown that the decay kinetics of TA spectra only become independent of the excitation fluence for excitation densities below 2×10^5 μm^{-3},[19] which for the DPT films we have investigated corresponds to a pump fluence of 1.3 $\mu J/cm^2$ at 500 nm. This value is more than an order of magnitude lower than the 31 $\mu J/cm^2$ fluence used to measure the data that appear in Figure 4B.

To determine if SSA strongly affects the TA spectra of DPT films, transient spectra were measured for a series of pump fluences. Figure 5 plots the decay of the S_1 induced absorption band at 421 nm measured in these experiments. As the intensity of the pump gradually increases, the rate of the singlet decay is found to accelerate. To highlight this effect, the inset of Figure 5 plots the amplitude of the S_1 induced absorption band at Δt = 20 ps as a function of the excitation fluence. This quantity scales sublinearly at high excitation fluence, indicating the presence of a quenching process whose amplitude depends on the initial singlet density, such as SSA. A similar scaling of the signal amplitude with excitation fluence can also result from pump-induced sample photodamage. However, the lack of hysteresis in the signal amplitude as the excitation fluence is cycled (Figure 5, inset, red ●) shows that the observed behavior does not result from sample damage. Plotted alongside the experimental data points are traces calculated from a kinetic model that accounts for the effects of SSA on the transient absorption signal and is described fully in section VII. This model predicts that the changes in the singlet population density resulting from SSA only become negligible for excitation densities below 2.1×10^5 μm^{-3},[62] a threshold density similar to that reported for polycrystalline tetracene films.[19] This limiting excitation density is roughly 3× smaller than that prepared in the lowest fluence TA experiments reported here (3.7 $\mu J/cm^2$), confirming that SSA needs to be accounted for when extracting the kinetics governing SF in disordered DPT films from these measurements.

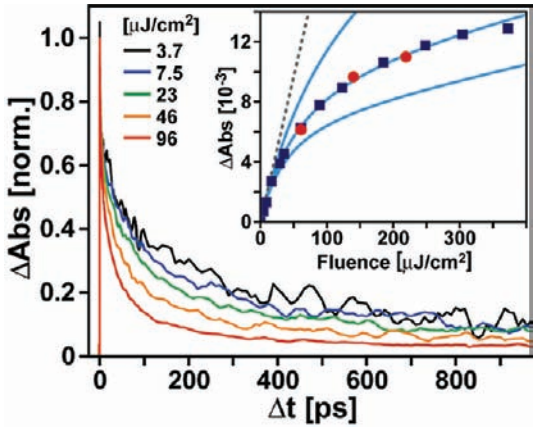

Figure 5. Normalized TA decay of the S_1-induced absorption at 421 nm measured at various excitation fluences for a vapor deposited DPT film. Inset: The amplitude of the induced absorption band at Δt = 20 ps plotted as a function of the excitation fluence. Red circles denote points measured after increasing the pump fluence to 370 $\mu J/cm^2$. The lack of hysteresis indicates that the sublinear scaling of the TA signal with the excitation fluence does not result from pump-induced film damage. The cyan lines represent the predicted signal amplitude based on the kinetic model that appears in section VII using singlet−singlet annihilation constants of $k_{SS} = 3.9 \times 10^{-9}$, 7.8×10^{-9}, and 1.2×10^{-8} cm^3/s in order of increasing curvature. The dashed gray line represents the signal amplitude predicted from the same model in the absence of exciton annihilation.

VI. TRACKING THE SINGLET AND TRIPLET POPULATIONS IN DPT FILMS

Retrieval of the kinetics that govern SF in amorphous DPT films from our measured TA and TCSPC data is complicated by the occurrence of SSA, the regeneration of singlet excitons stemming from triplet recombination, and spectral overlap between singlet- and triplet-induced absorption features, precluding the use of a single wavelength time trace to track the evolution of either the singlet or the triplet populations. In lieu of the construction of a kinetic model that attempts to describe each of these features at this point, we have instead elected to extract the time dependence of the singlet and triplet populations directly by fitting the DPT transient spectra as a linear combination of two basis spectra that represent the differential lineshapes characteristic of DPT's S_1 and T_1 states. These two spectra are determined experimentally from TA measurements independent of those performed on amorphous DPT films and are pictured in Figure 6A. The plotted basis spectra contain appropriately weighted negatively signed contributions from ground bleaching and stimulated emission in addition to positive features from absorption to higher lying states. How these spectra are obtained is outlined below.

The strong resemblance of the TA spectrum of vapor deposited DPT at short time delays to that of DPT in $CHCl_3$ indicates that transitions from DPT's S_1 state that fall in the visible spectral range are not strongly altered by the disordered film environment. This allows us to use the time-integrated transient spectrum of DPT in $CHCl_3$ to represent the basis spectrum of DPT's S_1 state. For the purposes of fitting the data, this spectrum has been red-shifted by the 280 cm^{-1} shift seen in ground-state absorption spectra (Figure 2B). Comparison of the amplitude of the ground-state bleach that appears in this spectrum with published extinction spectra of DPT's ground state[50] allows us to scale the amplitude of the basis spectrum such that it represents the change in the molar absorptivity of DPT following excitation to its S_1 state. In ref 33, it was demonstrated that the triplet extinction spectrum measured in nanosecond TA experiments of DPT in solution[50] gave a line shape nearly identical to those measured in our experiments on PtTPBP-doped DPT films. Thus, as the basis spectrum of DPT's T_1 state, we have used our previously measured DPT triplet spectrum scaled to match the amplitude of the extinction spectra of ref 50. Figure 6B compares the transient spectrum measured for a vapor deposited DPT film at a pump fluence of 7.5 $\mu J/cm^2$ with fits comprised of a linear combination of the S_1 and T_1 basis spectra in Figure 6A (see the Supporting Information for fits to other data sets). The agreement between the fit and the transient data is excellent, reproducing well both the decay of the $S_1 \rightarrow S_n$ transition at 421 nm and the growth of the $T_1 \rightarrow T_n$ transition near 485 nm.

dx.doi.org/10.1021/ja300504t | J. Am. Chem. Soc. 2012, 134, 6388−6400

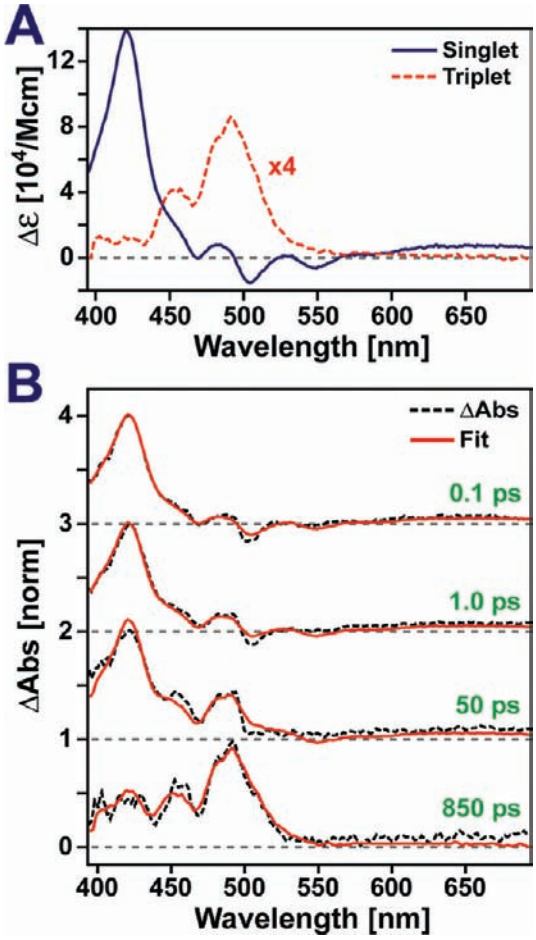

Figure 6. (A) Differential extinction spectra that denote the changes in the absorption profile of vapor deposited DPT films due to excitation of either DPT's lowest excited singlet or triplet state. (B) Comparison of TA spectra measured for vapor deposited DPT at a pump fluence of 7.5 μJ/cm^2 (black dashed) and a fit consisting of a linear combination of the singlet and triplet spectra in (A) (red).

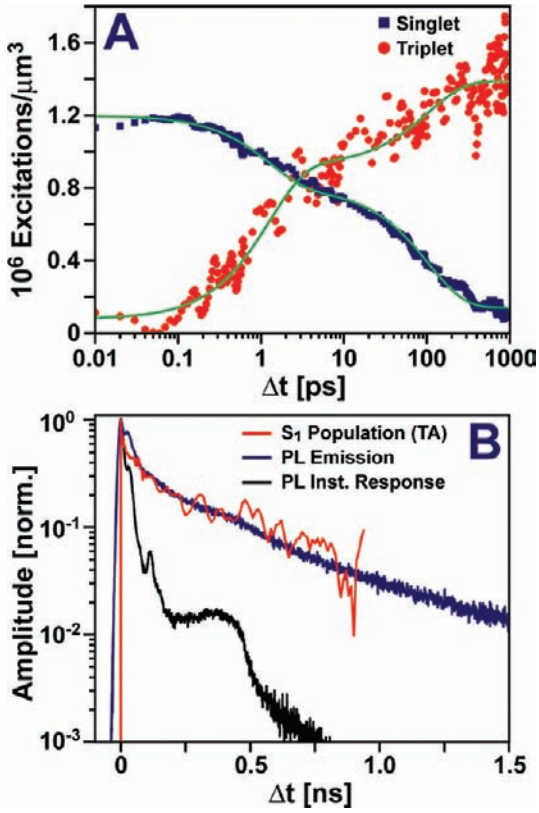

Figure 7. (A) Singlet (blue ■) and triplet (red ●) population densities determined from TA spectra of vapor deposited DPT measured at a pump fluence of 7.5 μJ/cm^2. The green lines denote a biexponential function that is included as a guide to the eye. (B) Comparison of the singlet population extracted from TA experiments (red) and the time-resolved fluorescence emission measured for a vapor deposited DPT film (blue). Other than a slight discrepancy at short delays due to the convolution of the emission with the instrument response of the TCSPC apparatus, both traces agree well, validating our fit procedure.

In addition to reproducing the data, the fits allow us to extract the time dependence of the S_1 and T_1 populations, which are plotted in Figure 7A. Perhaps the most striking feature present in the data is that the triplet population at 1 ns is ~1.2× larger than the initial singlet population, indicating that more than one triplet must be generated per singlet exciton. Because SF is the only mechanism by which the triplet population can exceed the initial singlet population, this result lends further support to our conclusion that SF occurs in amorphous DPT films. To verify that this finding is not a spurious result due to our chosen spectral decomposition procedure, Figure 7B compares the singlet population extracted from the DPT TA data set to a time-resolved emission scan collected for a vapor deposited film. Other than a slight discrepancy at short delay times due to the limited instrument response of the TCSPC apparatus (20 ps), both data sets overlay well, indicating that our fitting procedure predicts a rate of decay for the singlet population consistent with other experiments.

With our fitting procedure in hand, we can now estimate the SF yield for amorphous DPT films from our TA spectra by comparing the number of triplet excitons present in the film at long time delays to the initial singlet population. To remove contributions to our SF yield estimate that stem from exciton annihilation processes such as SSA, we have extracted the singlet and triplet populations from TA data measured over a range of excitation fluences. The results of this analysis appear in Figure 8, which plots the ratio of the triplet population density at a delay of 900 ps to the initial singlet density as a

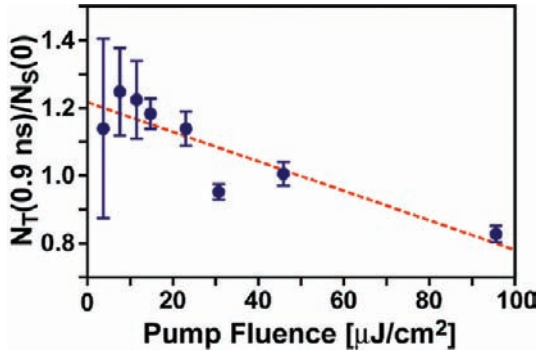

Figure 8. Ratio of triplet excitons observed at a time delay of 0.9 ns to the initial singlet population prepared in TA experiments as a function of the excitation fluence. Extrapolating to the annihilation free value (zero fluence) gives 1.22 triplets per singlet (61% SF yield). Error bars are based on one standard deviation in the values of the singlet and triplet populations extracted from the TA data.

dx.doi.org/10.1021/ja300504t | J. Am. Chem. Soc. 2012, 134, 6388−6400

function of excitation fluence. At all investigated fluences, the triplet-to-singlet ratio is quite high, ranging from 0.82 to 1.25 triplets per singlet (SF yields of 41−64.5%, respectively). At high excitation fluences, exciton annihilation provides an additional relaxation pathway that competes with SF, causing a decrease in the SF yield. However, in a photovoltaic functioning under solar irradiation, the steady-state singlet and triplet populations are expected to be orders of magnitude smaller than those prepared in the TA experiments described here. Given that the SF yield appears to vary linearly with excitation fluence, we have extrapolated the yield to zero fluence to obtain a value more representative of a DPT film under solar illumination. This yields a value of 1.22 produced triplets per singlet exciton (61% SF yield), which is surprisingly large given the absence of structural order in our DPT films. While this value falls short of the ∼200% triplet yield reported for polycrystalline tetracene,[18] it compares favorably with yields reported for other polycrystalline materials. This includes films of 6,13-bis(triisopropylsilylethynyl)-pentacene, for which a 144% triplet yield was observed,[12] and 1,3-diphenylisobenzofuran, which displays a 125% triplet yield at 300 K that increases to 200% at 77 K.[24] Moreover, we note that the SF yield we calculate for DPT is likely a slight underestimate. Because of the current limitations of our TA apparatus, we are limited to probing delay times less than 1 ns. However, at this time delay, the singlet and triplet populations have not finished evolving, as evidenced by the TCSPC data that continue to decay beyond 1 ns. If we assume that the residual singlet population in our TA spectra at a delay of 1 ns exclusively decays via SF, this increases the number of triplets produced per singlet to 1.40 (70% SF yield).

VII. A SIMPLE KINETIC MODEL FOR SF IN DISORDERED FILMS

Returning to the singlet and triplet populations shown in Figure 7A, the decay of the S_1 state and corresponding rise of the T_1 state occur over two principal time ranges, with ∼50% of the population evolution occurring within 3 ps and the remaining triplet production occurring over the course of ∼100 ps. As a guide to the eye, a biexponential with time constants of 1.3 and 105 ps is superimposed on top of the data. In polycrystalline acene films, TA experiments generally identify a single primary rate for SF.[17,18,23] However, given that the SF rate is expected to depend intimately on the relative geometry and distance between neighboring chromophores,[9,30,31,63] in a disordered film such as those formed by DPT it seems likely that some neighboring chromophores will be oriented in geometries that promote SF, while other molecular pairs will adopt configurations that present a significant energetic barrier to SF.

Figure 9 provides an illustration of one of the simpler kinetic models that can account for triplet production over two time scales. This model assumes that due to structural disorder, only a subset of the neighboring DPT molecular pairs within the film are capable of undergoing SF. After photoexcitation, singlet excitons created near these pairs can fission rapidly, leading to an initial exponential burst phase of triplet production. Meanwhile, singlets created at other locations within the film can diffuse via Förster energy transfer to these pairs, yielding a secondary, diffusion-limited triplet production phase. Provided that the film is on average spatially homogeneous and the number of SF sites is small as compared to the initial singlet

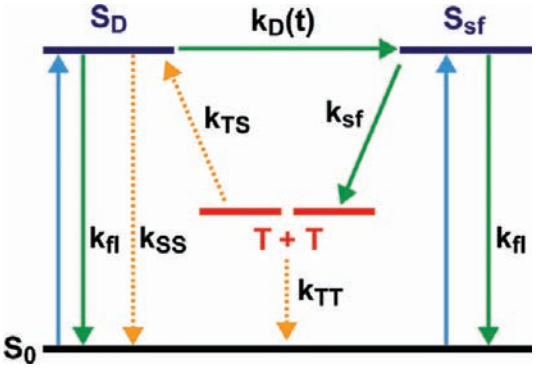

Figure 9. Illustration of the energy transfer and relaxation processes used to model the kinetics of SF in amorphous DPT films. Light absorption is denoted by cyan arrows, single exciton transfer and relaxation processes by green arrows, and exciton annihilation processes by orange dashed arrows.

population, the rate at which singlets encounter SF sites is given by the Smoluchowski theory of diffusion-limited reactions:[64,65]

$$k_D(t) = 4\pi R D c_{sf}\left(1 + \frac{R}{\sqrt{\pi D t}}\right) \quad (1)$$

In eq 1, D denotes the singlet exciton diffusion constant, c_{sf} is the concentration of SF sites within the film, and R denotes the maximum distance a singlet can be from a SF site and undergo SF. Accounting for variations in energy transfer rate due to disorder[66] is beyond the scope of the current model.

With eq 1 in hand, it is possible to write a set of coupled rate equations for the interchange of singlet and triplet populations within the film:

$$\begin{aligned}
\frac{d[S_{sf}]}{dt} &= -(k_{fl} + k_{SF})[S_{sf}] + k_D(t)[S_D] \\
\frac{d[S_D]}{dt} &= -k_{fl}[S_D] - k_D(t)[S_D] - k_{SS}[S_D]^2 + k_{TS}[T]^2 \\
\frac{d[T]}{dt} &= 2k_{sf}[S_{sf}] - k_{TS}[T]^2 - k_{TT}[T]^2
\end{aligned} \quad (2)$$

The above set of equations divides the singlet population between singlets that occupy SF sites, S_{sf}, and those that do not, S_D. S_{sf} can decay via singlet fission (k_{sf}), producing two triplets, or through other pathways such as fluorescence, internal conversion, and intersystem crossing. These latter processes are accounted for by the sum of their rates, k_{fl}. Because the intersystem crossing rate in isolated DPT has been shown to be quite long ($1/k_{ISC}$ = 89 ns)[50] as compared to the subnanosecond time scales probed in our TA experiments, the production of triplets through intramolecular intersystem crossing is neglected in our model. S_{sf} can be regenerated by the diffusion of S_D to SF sites as dictated by the time-dependent rate, $k_D(t)$, given by the Smoluchowski theory. As with S_{sf}, S_D can also decay via the same nontriplet producing pathways described by k_{fl}. As an initial condition for our model, we assume that the starting population of S_{sf} is given by δS_o, where S_o is the total population of singlets prepared by the excitation pulse and δ is a parameter that varies between zero and one and is floated to fit the data. The corresponding initial population of S_D is $(1 - \delta)S_o$.

dx.doi.org/10.1021/ja300504t | J. Am. Chem. Soc. 2012, 134, 6388−6400

Similar to kinetic models used to describe SF in tetracene crystals,[18,60] we allow the singlet population to decay through SSA, whose rate is given by k_{SS}. The triplet population can also decay through exciton annihilation, but a subset of these bimolecular recombination processes can lead to the regeneration of singlet excitons.[8] We account for these two possibilities through the inclusion of two terms, k_{TS} and k_{TT}, which describe triplet−triplet annihilation events that generate a singlet exciton (k_{TS}) and those that do not (k_{TT}). For simplicity, we assume that triplet−triplet annihilation occurs between uncorrelated triplet pairs away from SF sites. Correspondingly, these annihilation events only populate S_D within our model, not S_{sf}.

To model our experimental TA spectra, eq 2 was integrated numerically using a Runge−Kutta method in Matlab software to yield the singlet and triplet populations as a function of time. These populations were then used in conjunction with the extinction spectra in Figure 6A to reconstruct the TA data, and a least-squares minimization routine was used to optimize the values of the rate coefficients in eq 2 as well as the initial ratio between S_{sf} and S_D. Because $k_D(t)$ contains three unknowns, c_{SF}, R, and D, but only two of these terms are independent, for the purposes of fitting eq 2, $k_D(t)$ was parametrized as $k_D(t) = a + bt^{-1/2}$, with a and b as free parameters. To self-consistently account for exciton annihilation, this fit was performed simultaneously to multiple TA data sets recorded for excitation fluences ranging from 3.7 to 96 μJ/cm^2, with only the initial singlet population density allowed to vary between fits to individual data sets. The best-fit parameters determined from the model are listed in Table 1, and a full comparison of the model and experimental TA spectra appears in the Supporting Information.

Table 1. Best-Fit Parameters for the Kinetic Model Described in Section VII[a]

parameter	best-fit value
$1/k_{sf}$	0.8 ps
a	1.9×10^{-3} ps^{-1}
b	1.2×10^{-2} ps$^{-1/2}$
k_{SS}	3.9×10^{-9} cm^3/s
k_{TT}	9.0×10^{-11} cm^3/s
k_{TS}	4.6×10^{-11} cm^3/s
δ	0.33
R	4.3 Å
D	1.5×10^{-5} cm^2/s

[a]For fitting purposes, $k_D(t)$ was parameterized as $a + bt^{-1/2}$. δ denotes the percentage of the initial singlet population that contributes to S_{sf}. Values for R and D are calculated from the best-fit values for a and b under the assumption that the singlet fission site concentration, c_{sf}, in eq 1 is given by $\delta c_{DPT}/2$, where c_{DPT} is the concentration of DPT molecules in the film.

To indicate the quality of our model, Figure 10 shows a comparison of the singlet and triplet populations predicted by the model with those extracted by the fitting procedure described in section VI. While the agreement is not perfect, the model shows good qualitative agreement with the data, capturing well the decay of the singlet population and showing a growth of the triplet population over multiple time scales. However, the model does not properly reproduce the amplitude of the triplet population measured in experiments at high excitation fluence. This shortcoming likely stems from

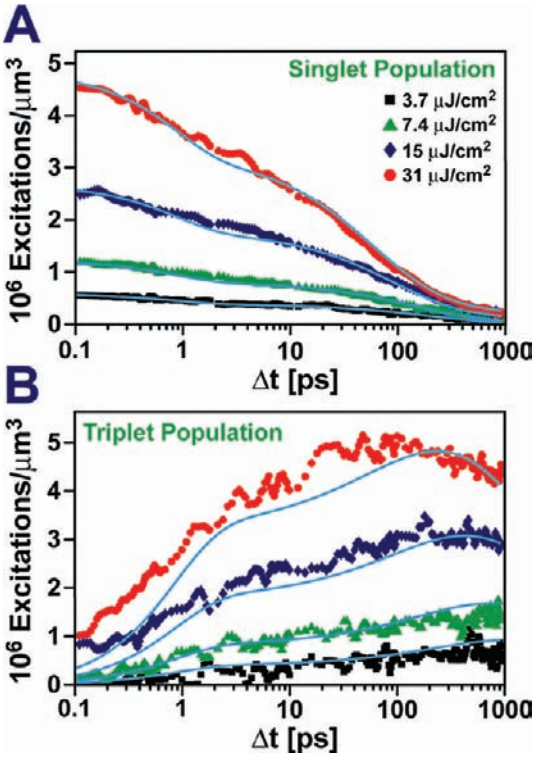

Figure 10. Singlet (A) and triplet (B) populations extracted from TA experiments performed at a series of excitation fluences as compared to populations calculated on the basis of the kinetic model described in section VII of the text. A simultaneous fit to all pictured data sets was performed.

the model's use of time-independent rate coefficients to describe exciton annihilation processes, which neglects diffusive contributions to these events,[29,67] as well as triplet exciton trapping at impurities in the film. This causes the fits to overestimate the amount of triplet−triplet annihilation that occurs at long delays, which is most evident in the data sets measured at high excitation fluence. Similar effects cause the best-fit value of k_{SS} to differ from the value that gives the best agreement with the intensity scaling of the $S_1 \rightarrow S_n$ induced absorption feature at 421 nm (Figure 5, inset). While the agreement between the model and the experimental data is lacking at high excitation fluence, it improves as the excitation density is lowered and effects due to exciton annihilation are suppressed. In the Supporting Information, we show that the model reproduces 99% of the singlet exciton decay observed in the time-resolved fluorescence measurements shown in Figure 3, which are measured for excitation densities 1−2 orders of magnitude smaller than those used in TA measurements.

Despite the poor treatment of triplet exciton annihilation by the kinetic model, it is nonetheless instructive to compare its best-fit parameters to those that have been reported for tetracene and pentacene films. The SF time scale of 0.8 ps that we measure for DPT films is more than an order of magnitude faster than the ∼40−90 ps time scales that have been reported for tetracene films,[11,17,19] but is markedly slower than the 80 fs fission rate measured for pentacene films.[10,22,23] In part, the increase in the SF rate moving from tetracene to pentacene can be rationalized on the basis of the value of $2E(T_1) - E(S_1)$ for these materials, which correlates with the thermodynamic driving force for SF.[27] For tetracene, $2E(T_1) - E(S_1) = 0.19-0.24$ eV,[20−22] indicating that SF requires thermal activation,

dx.doi.org/10.1021/ja300504t | J. Am. Chem. Soc. 2012, 134, 6388−6400

while in pentacene $2E(T_1) - E(S_1) = -0.11$ eV,[22] suggesting the potential for barrierless fission. Indeed, measurements by Thorsmølle et al.[11] have shown that the formation of triplets in tetracene single crystals displays a pronounced temperature dependence indicative of an activation barrier of 70 meV, while SF in pentacene single crystals is independent of temperature. While to the best of our knowledge, measurements of the absolute S_1 and T_1 energies of DPT in a film environment have not been made, the values of these quantities in benzene solution give a value of −87 meV for $2E(T_1) - E(S_1)$,[50] suggesting that similar to pentacene, SF between two properly arranged DPT monomers may not require a large activation energy.

Additional information regarding the driving force for SF in DPT films as compared to films of other acenes can be obtained by analyzing the rate at which singlet excitons are regenerated by triplet−triplet annihilation (k_{TS}). As the reverse reaction of SF, contributions to the measured kinetics that stem from triplet−triplet annihilation are expected to be suppressed as $2E(T_1) - E(S_1)$ decreases. Using a model that treats exciton annihilation using time-independent rate coefficients, Burdett et al.[18] found that a value of $k_{TS} = 5.0 \times 10^{-10}$ cm^2/s qualitatively reproduced time-resolved emission measurements of tetracene films. In contrast, the value of k_{TS} we extract from our model for DPT films is roughly 10× smaller. This observation taken together with the fact that our model overestimates the degree to which triplet annihilation occurs shows that triplet annihilation is suppressed in DPT films relative to tetracene and suggests that DPT possesses a larger thermodynamic driving force for SF. This finding is consistent with those of a recent time-resolved emission study of rubrene crystals, which concluded that the value of $2E(T_1) - E(S_1)$ is nearly zero for rubrene.[51] Upon transitioning from solution to a thin film environment, the S_1 energy of tetracene molecules is reduced by interchromophore coupling, leading to a red shift of its optical spectra (Figure 2A). In contrast, the phenyl rings of DPT afford a larger spacing between neighboring molecules in thin films that reduces interchromophore coupling. This leads to a higher S_1 energy for DPT relative to tetracene in thin films,[68] which may be capable of undergoing exergonic SF.

In our model, we have not included an intermediate state to which the singlet exciton first transitions before it fissions to two triplets. Both charge transfer[63] and neutral intermediate states[30,31] have been postulated on the basis of theoretical calculations. Recent time-resolved two-photon photoemission experiments have observed an intermediate state preceding fission in pentacene, but with a relatively short lifetime of 260 ± 50 fs.[69] In modeling the presented TA data, we have found that the addition of an intermediate state to the rate equations given in eq 2 does not significantly improve the quality of the fit. However, given the short lifetime expected for such a state,[69] a difference in the rates with which the photoexcited singlet population decays and the triplet population rises due to the presence of an intermediate state may fall within experimental error. While our model does not need to account for an intermediate state that precedes fission to model the presented TA and TCSPC data sets, this does not rule out the possibility for the existence of such a state.

One interesting and surprising result predicted by our model is that one-third of the initial singlet population is created at sites capable of undergoing SF, suggesting an appreciable concentration of these sites in the film despite its high degree of conformational disorder. One possible explanation for this observation is that a large number of DPT molecules form dimer pairs with their π-systems in close proximity, but still possess enough conformational disorder to not impose any long-range ordering of the film. An estimate of the separation between the two molecules within the dimer pair as well as the rate at which singlet excitons diffuse within the film can be obtained from the parameters that comprise $k_D(t)$. If we assume that the SF site concentration, c_{sf}, is described by $\delta c_{DPT}/2$, where c_{DPT} is the concentration of DPT molecules in the film (2.4 M based on optical absorption measurements), then the resulting values of the singlet diffusion constant, D, and SF encounter radius, R, are 1.5×10^{-5} cm^2/s and 4.3 Å, respectively. Using the procedure outlined by Rand et al.,[70] it is possible to calculate D from DPT's self-transfer Forster radius, R_0, which we have calculated using the PhotochemCAD software package,[71] which predicts self-transfer radii for many acenes in good agreement with prior reported values (i.e., anthracene, 2.3 nm calculated, 2.2 nm reported;[72] perylene, 4.0 nm calculated, 3.8 nm reported[72]). For DPT, we calculate a R_0 value of 3.3 nm, which in turn yields $D = 1.4 \times 10^{-4}$ cm^2/s, a value that is an order of magnitude larger than that extracted from our kinetic model. Given the high degree of disorder in our vapor deposited DPT films, it is likely that they contain some low energy exciton traps that can immobilize diffusing excitons,[29,73] leading to the low diffusion constant predicted by our model. Such trap sites may provide additional avenues for nonradiative decay, resulting in the less than 200% triplet yield we observe in our transient spectra. Interestingly, the extracted value of R is small as compared to the average distance between molecules, 10.9 Å, calculated on the basis of the film's concentration, suggesting that SF dimer pairs are sites where molecules closely associate. This value of R closely matches the spacing between pentacene dimers predicted by ab initio calculations to allow a nonadiabatic transition between the lowest excited singlet exciton of the pair to a dark state that induces SF.[30]

We look to the crystal structure of DPT to gain insight into what these dimer pairs may resemble. The single crystal structure of DPT has been reported by Kitamura et al. for crystals grown from xylene solvent.[74] We have also grown DPT crystals and determined their structure (Figure 11, see the Supporting Information for additional details). However, our crystals were grown by vacuum sublimation, similar to the process used for thin film deposition, but at a much slower growth rate than that used to prepare the disordered films investigated above. The molecular structure of the tetracence core reported by Kitamura et al. is quite similar to that of the vacuum sublimed crystals we have examined. Fourteen of the carbons (C5−C18) of the DPT molecules in the vapor grown crystals lie within 0.08 Å of a least-squares plane. The remaining four carbons are bent up from this plane, by up to 0.37 Å. A similar structure is observed for DPT molecules in crystals obtained from xylene.[74] The principal difference between the structure reported by Kitamura et al. and the one we report here is the orientation of the DPT phenyl rings (Figure 12). In the sublimed crystals, both phenyl rings are twisted in the same direction, with a dihedral angle of 70°. In contrast, the phenyl groups of the xylene crystallized materials are canted in opposite directions, with dihedral angles of 75° and 94°.

Unlike crystals of tetracene, which adopt a herringbone arrangement that places the π-systems of neighboring molecules at an angle of 51° to one another,[75,76] the packing of DPT involves cofacial stacking of the DPT molecules along

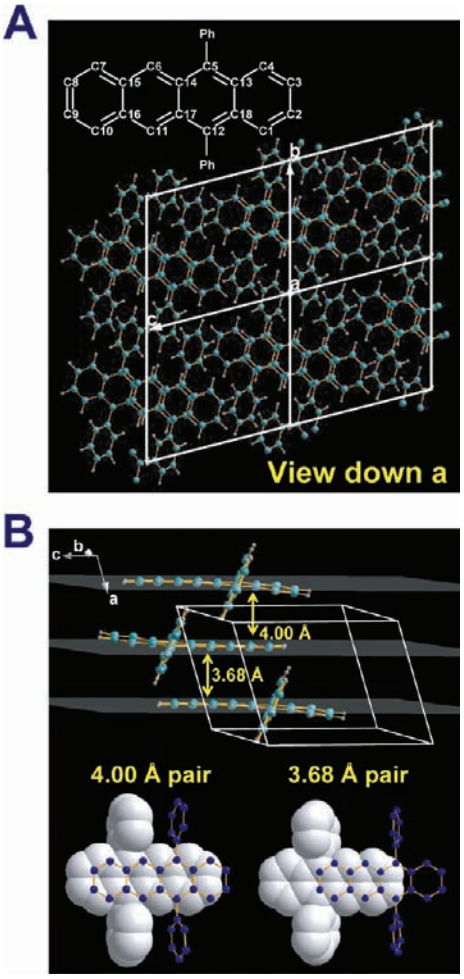

Figure 11. Structure of vapor grown DPT crystals determined from powder X-ray diffraction experiments. (A) View looking down the crystal's *a*-axis, showing that DPT molecules prefer to stack in a cofacial arrangement. (B) The spacing between neighboring molecules along the *a*-axis alternates between eclipsed and staggered arrangements with respective spacings of 4.00 and 3.68 Å.

the crystal's *a*-axis (Figure 11A). Both the sublimed and the xylene crystallized samples have similar molecular packing in this respect, but their unit cell parameters differ to some extent, with the unit cell volume of the vapor grown crystals being slightly less (973 Å^3) than those isolated from xylene (985 Å^3). DPT molecules alternate between being eclipsed and staggered along the *a*-axis (Figure 11B). For eclipsed neighbors, the phenyl groups of both DPT molecules prevent close approach of the tetracene cores, but this does not occur for staggered configurations. We estimate the intermolecular spacing for the DPT molecules by considering their C5−C18 planes. For both xylene and vapor grown crystals, the spacing of the tetracene cores in eclipsed configurations is 4.00 Å, while the spacing in staggered configurations is somewhat smaller, 3.82 Å for xylene grown crystals and 3.68 Å for vapor grown crystals. The decreased spacing for the vapor grown crystals partly explains the lower cell volume and is likely due to less severe steric interactions for the DPT phenyl groups in the vapor grown sample.

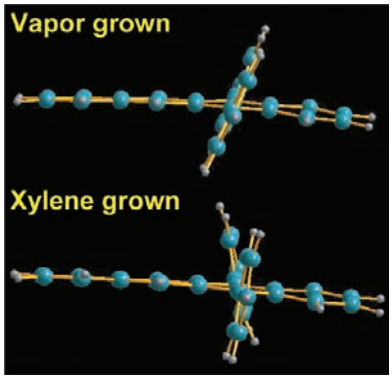

Figure 12. Comparison of the structure of individual DPT molecules in vapor grown crystals and crystals grown from xylene solution.[74] While the phenyl rings of DPT molecules in vapor grown crystals are canted in the same direction, they are tilted in opposite directions in the structure obtained from xylene grown crystals, leading to a slightly larger unit cell volume for this latter structure.

Factors dictating the ideal geometry for SF have been discussed by Greyson et al.[77] who note that π-stacking between neighboring chromophores represents a fundamental balance between competing effects. While π-stacking leads to improved interchromophore coupling, this can also lower the energy of the lowest excited singlet state, potentially making SF endergonic. This has led to the suggestion that neighboring chromophores with slip-stacked geometries may be favorable candidates for SF.[6] DPT crystals thus represent an interesting test case for SF because their structure alternates between staggered and eclipsed π-systems. Unfortunately, we have as yet been unable to obtain high-quality crystals that are suitable for time-resolved studies, preventing a direct comparison of the excited-state properties of DPT crystals to those we report here for disordered films. However, we find that the SF encounter radius from our model, 4.3 Å, closely approximates the spacing between both neighboring eclipsed and staggered molecules along the *a*-axis, suggesting that regions of the film where two molecules arrange themselves in a cofacial manner can undergo efficient SF.

VIII. CONCLUSIONS

We have used a combination of ultrafast TA and time-resolved emission measurements to characterize the morphology and excited-state dynamics of vapor deposited DPT films. While XRD and TEM measurements confirm that these films are largely amorphous, we nonetheless observe that upward of 61% of the singlet excitons created by photoexcitation fission to a pair of triplet excitons. Triplet production occurs over two principal time scales, with approximately one-half of the triplets appearing with an exponential time scale of 0.8 ps followed by a slower phase of triplet growth over the course of ∼100 ps. This behavior is consistent with a model that assumes that only certain locations in the disordered film adopt a configuration suitable for SF, leading to the diffusive production of triplets at these sites.

Within the larger context of SF-based photovoltaics, our results are highly encouraging because they suggest that SF may be achievable in films of low crystalline quality, relaxing constraints placed on the film manufacturing process. Despite these positive results, however, much work remains to be done to achieve low-cost, high efficiency SF-based OPVs. In particular, it is still not understood how the properties of a SF absorber are affected by the presence of a complementary long-wavelength absorber, which is needed to achieve devices capable of circumventing the Shockley−Queisser limit.[5]

dx.doi.org/10.1021/ja300504t | J. Am. Chem. Soc. 2012, 134, 6388−6400

Experiments are underway to investigate how the energy transfer pathways that operate in DPT films are modified in the presence of a complementary absorber.

■ ASSOCIATED CONTENT

Supporting Information

Additional details related to the fitting procedure utilized in section VI to extract the singlet and triplet populations from TA data as well as a more detailed comparison of observables calculated using the kinetic model described in section VII with experiment. A table of the unit cell parameters for the DPT crystal structure. This material is available free of charge via the Internet at http://pubs.acs.org.

■ AUTHOR INFORMATION

Corresponding Author

met@usc.edu; stephen.bradforth@usc.edu

Present Address

‡Department of Chemistry, Carleton College, Northfield, Minnesota 55057, United States.

Notes

The authors declare no competing financial interest.

■ ACKNOWLEDGMENTS

This material is based upon work supported through the Center for Energy Nanoscience, an Energy Frontier Research Center funded by the U.S. Department of Energy, Office of Science, Office of Basic Energy Sciences (DE-SC0001013). S.T.R. thanks the National Science Foundation for support from an ACC-F fellowship (CHE-0937015) as well as Saptaparna Das and Anirban Roy for their aid in performing time-resolved photoluminescence measurements. J.N.M. would like to acknowledge support from a summer undergraduate research fellowship sponsored in part by the National Science Foundation. X-ray diffraction measurements were carried out using an instrument secured through a grant from the National Science Foundation (CRIF-1048807).

■ REFERENCES

(1) Shockley, W.; Queisser, H. J. *J. Appl. Phys.* **1961**, *32*, 510−519.
(2) Klimov, V. I. *Annu. Rev. Phys. Chem.* **2007**, *58*, 635−673.
(3) Beard, M. C. *J. Phys. Chem. Lett.* **2011**, *2*, 1282−1288.
(4) Sambur, J. B.; Novet, T.; Parkinson, B. A. *Science* **2010**, *330*, 63−66.
(5) Hanna, M. C.; Nozik, A. J. *J. Appl. Phys.* **2006**, *100*, 074510.
(6) Smith, M. B.; Michl, J. *Chem. Rev.* **2010**, *110*, 6891−6936.
(7) Singh, S.; Jones, W. J.; Siebrand, W.; Stoicheff, B. P.; Schneider, W. G. *J. Chem. Phys.* **1965**, *42*, 330−342.
(8) Merrifield, R. E. *Pure Appl. Chem.* **1971**, *27*, 481−498.
(9) Müller, A. M.; Avlasevich, Y. A.; Schoeller, W. W.; Müllen, K.; Bardeen, C. J. *J. Am. Chem. Soc.* **2007**, *129*, 14240−14250.
(10) Rao, A.; Wilson, M. W. B.; Hodgkiss, J. M.; Albert-Seifried, S.; Bässler, H.; Friend, R. H. *J. Am. Chem. Soc.* **2010**, *132*, 12698−12703.
(11) Thorsmølle, V. K.; Averitt, R. D.; Demsar, J.; Smith, D. L.; Tretiak, S.; Martin, R. L.; Chi, X.; Crone, B. K.; Ramirez, A. P.; Taylor, A. J. *Phys. Rev. Lett.* **2009**, *102*, 017401.
(12) Ramanan, C.; Smeigh, A. L.; Anthony, J. E.; Marks, T. J.; Wasielewski, M. R. *J. Am. Chem. Soc.* **2012**, *134*, 386−397.
(13) Lanzani, G.; Stagira, S.; Cerullo, G.; Silvestri, S. D.; Comoretto, D.; Moggio, I.; Cuniberti, C.; Musso, G. F.; Dellepiane, G. *Chem. Phys. Lett.* **1999**, *313*, 525−532.
(14) Lanzani, G.; Cerullo, G.; Zavelani-Rossi, M.; Silvestri, S. D.; Comoretto, D.; Musso, G.; Dellepiane, G. *Phys. Rev. Lett.* **2001**, *87*, 187402.
(15) Guo, J.; Ohkita, H.; Benten, H.; Ito, S. *J. Am. Chem. Soc.* **2009**, *131*, 16869−16880.
(16) Wang, C.; Tauber, M. J. *J. Am. Chem. Soc.* **2010**, *132*, 13988−13991.
(17) Grumstrup, E. M.; Johnson, J. C.; Damrauer, N. H. *Phys. Rev. Lett.* **2010**, *105*, 257403.
(18) Burdett, J. J.; Muller, A. M.; Gosztola, D.; Bardeen, C. J. *J. Chem. Phys.* **2010**, *133*, 144506.
(19) Burdett, J. J.; Gosztola, D.; Bardeen, C. J. *J. Chem. Phys.* **2011**, *135*, 214508.
(20) Groff, R. P.; Avakian, P.; Merrifield, R. E. *Phys. Rev. B* **1970**, *1*, 815−817.
(21) Tomkiewicz, Y.; Groff, R. P.; Avakian, P. *J. Chem. Phys.* **1971**, *54*, 4504.
(22) Jundt, C.; Klein, G.; Sipp, B.; Moigne, J. L.; Joucla, M.; Villaeys, A. A. *Chem. Phys. Lett.* **1995**, *241*, 84−88.
(23) Wilson, M. W. B.; Rao, A.; Clark, J.; Kumar, R. S. S.; Brida, D.; Cerullo, G.; Friend, R. H. *J. Am. Chem. Soc.* **2011**, *133*, 11830−11833.
(24) Johnson, J. C.; Nozik, A. J.; Michl, J. *J. Am. Chem. Soc.* **2010**, *132*, 16302−16303.
(25) Lee, J.; Jadhav, P.; Baldo, M. A. *Appl. Phys. Lett.* **2009**, *95*, 033301.
(26) Jadhav, P. J.; Mohanty, A.; Sussman, J.; Lee, J.; Baldo, M. A. *Nano Lett.* **2011**, *11*, 1495−1498.
(27) Paci, I.; Johnson, J. C.; Chen, X.; Rana, G.; Popovic, D.; David, D. E.; Nozik, A. J.; Ratner, M. A.; Michl, J. *J. Am. Chem. Soc.* **2006**, *128*, 16546−16553.
(28) Marciniak, H.; Fiebig, M.; Huth, M.; Schiefer, S.; Nickel, B.; Selmaier, F.; Lochbrunner, S. *Phys. Rev. Lett.* **2007**, *99*, 176402.
(29) Marciniak, H.; Pugliesi, I.; Nickel, B.; Lochbrunner, S. *Phys. Rev. B* **2009**, *79*, 235318.
(30) Zimmerman, P. M.; Zhang, Z.; Musgrave, C. B. *Nat. Chem.* **2010**, *2*, 648−652.
(31) Zimmerman, P. M.; Bell, F.; Casanova, D.; Head-Gordon, M. *J. Am. Chem. Soc.* **2011**, *133*, 19944−19952.
(32) Shaheen, S. E.; Radspinner, R.; Peyghambarian, N.; Jabbour, G. E. *Appl. Phys. Lett.* **2001**, *79*, 2996−2998.
(33) Roberts, S. T.; Schlenker, C. W.; Barlier, V.; McAnally, R. E.; Zhang, Y.; Mastron, J. N.; Thompson, M. E.; Bradforth, S. E. *J. Phys. Chem. Lett.* **2011**, *2*, 48−54.
(34) Anthony, J. E.; Eaton, D. L.; Parkin, S. R. *Org. Lett.* **2002**, *4*, 15−18.
(35) Barlier, V. S.; Schlenker, C. W.; Chin, S. W.; Thompson, M. E. *Chem. Commun.* **2011**, *47*, 3754−3756.
(36) Milita, S.; Servidori, M.; Cicoira, F.; Santato, C.; Pifferi, A. *Nucl. Instrum. Methods Phys. Res., Sect. B* **2006**, *246*, 101−105.
(37) Klevens, H. B.; Platt, J. R. *J. Chem. Phys.* **1949**, *17*, 470−481.
(38) Tanaka, J. *Bull. Chem. Soc. Jpn.* **1965**, *38*, 86−103.
(39) Malkin, J. *Photophysical and Photochemical Properties of Aromatic Compounds*; CRC Press: Boca Raton, FL, 1992.
(40) Cicoira, F.; Santato, C.; Dinelli, F.; Murgia, M.; Loi, M. A.; Biscarini, F.; Zamboni, R.; Heremans, P.; Muccini, M. *Adv. Funct. Mater.* **2005**, *15*, 375−380.
(41) Shao, Y.; Sista, S.; Chu, C.-W.; Sievers, D.; Yang, Y. *Appl. Phys. Lett.* **2007**, *90*, 103501.
(42) Schlosser, D. W.; Philpott, M. R. *Chem. Phys.* **1980**, *49*, 181−199.
(43) Yamagata, H.; Norton, J.; Hontz, E.; Olivier, Y.; Beljonne, D.; Brédas, J. L.; Silbey, R. J.; Spano, F. C. *J. Chem. Phys.* **2011**, *134*, 204703.
(44) Spano, F. C. *Acc. Chem. Res.* **2010**, *43*, 429−439.
(45) Spano, F. C. *Annu. Rev. Phys. Chem.* **2006**, *57*, 217−243.
(46) Lim, S.-H.; Bjorklund, T. G.; Spano, F. C.; Bardeen, C. J. *Phys. Rev. Lett.* **2004**, *92*, 107402.
(47) Tavazzi, S.; Borghesi, A.; Papagni, A.; Spearman, P.; Silvestri, L.; Yassar, A.; Camposeo, A.; Polo, M.; Pisignano, D. *Phys. Rev. B* **2007**, *75*, 245416.
(48) Johnson, R. C.; Merrifield, R. E. *Phys. Rev. B* **1970**, *1*, 896−902.

(49) Ern, V.; Saint-Clair, J. L.; Schott, M.; Delacote, G. *Chem. Phys. Lett.* **1971**, *10*, 287−290.
(50) Burgdorff, C.; Kircher, T.; Löhmannsröben, H.-G. *Spectrochim. Acta, Part A* **1988**, *44A*, 1137−1141.
(51) Ryasnyanskiy, A.; Biaggio, I. *Phys. Rev. B* **2011**, *84*, 193203.
(52) Similar to DPT's steady-state absorption spectra (Figure 2B), we observe a slight red-shift of the peak of the $S_1 \rightarrow S_n$ transition going from $CHCl_3$ solution to a vapor deposited film. This slight shift likely results from a change in the dielectric environment surrounding DPT molecules.
(53) Bensasson, R.; Land, E. J. *Trans. Faraday Soc.* **1971**, *67*, 1904−1915.
(54) Burgdorff, C.; Löhmannsröben, H.-G. *J. Lumin.* **1994**, *59*, 201−208.
(55) Nijegorodov, N.; Ramachandran, V.; Winkoun, D. P. *Spectrochim. Acta, Part A* **1997**, *53*, 1813−1824.
(56) Schwieger, T.; Liu, X.; Olligs, D.; Knupfer, M.; Schmidt, T. *J. Appl. Phys.* **2004**, *96*, 5596−5600.
(57) Schiefer, S.; Huth, M.; Dobrinevski, A.; Nickel, B. *J. Am. Chem. Soc.* **2007**, *129*, 10316−10317.
(58) Rao, A.; Wilson, M. W. B.; Albert-Seifried, S.; Pietro, R. D.; Friend, R. H. *Phys. Rev. B* **2011**, *84*, 195411.
(59) Note that, due to overlap between the absorption profiles of DPT's T_1 and S_0 states, this latter TA spectrum represents the equally weighted sum of a positively signed $T_1 \rightarrow T_n$ absorption signal and a negatively signed photobleach of DPT's ground-state absorption. Because the molar absorptivity of the $T_1 \rightarrow T_n$ transition is ∼3× greater than that of the $S_0 \rightarrow S_1$ transition, DPT's T_1 TA spectrum is net positive.
(60) Fleming, G. R.; Millar, D. P.; Morris, G. C.; Morris, J. M.; Robinson, G. W. *Aust. J. Chem.* **1977**, *30*, 2353−2359.
(61) Campillo, A. J.; Hyer, R. C.; Shapiro, S. L.; Swenberg, C. E. *Chem. Phys. Lett.* **1977**, *48*, 495−500.
(62) This threshold value is calculated by comparing the singlet population integrated over the course of 1 ns predicted by the model in section VII in the presence and absence of exciton annihilation. At an excitation density of $2.1 \times 10^5\ \mu m^{-3}$, these two quantities differ by less than 5%.
(63) Greyson, E. C.; Vura-Weis, J.; Michl, J.; Ratner, M. A. *J. Phys. Chem. B* **2010**, *114*, 14168−14177.
(64) Powell, R. C.; Soos, Z. G. *J. Lumin.* **1975**, *11*, 1−45.
(65) Rice, S. A. *Diffusion-Limited Reactions*; Elsevier: Amsterdam, 1985; Vol. *25*.
(66) Johnson, J. M.; Chen, R.; Chen, X.; Moskun, A. C.; Zhang, X.; Hogen-Esch, T. E.; Bradforth, S. E. *J. Phys. Chem. B* **2008**, *112*, 16367−16381.
(67) Engel, E.; Leo, K.; Hoffmann, M. *Chem. Phys.* **2006**, *325*, 170−177.
(68) Schlenker, C. W.; Barlier, V. S.; Chin, S. W.; Whited, M. T.; McAnally, R. E.; Forrest, S. R.; Thompson, M. E. *Chem. Mater.* **2011**, *23*, 4132−4140.
(69) Chan, W.-L.; Ligges, M.; Jailaubekov, A.; Kaake, L.; Miaja-Avila, L.; Zhu, X.-Y. *Science* **2011**, *334*, 1541−1545.
(70) Lunt, R. R.; Giebink, N. C.; Belak, A. A.; Benziger, J. B.; Forrest, S. R. *J. Appl. Phys.* **2009**, *105*, 053711.
(71) Dixon, J. M.; Taniguchi, M.; Lindsey, J. S. *Photochem. Photobiol.* **2005**, *81*, 212−213.
(72) Berlman, I. B. *Energy Transfer Parameters of Aromatic Compounds*; Academic Press: New York, 1973.
(73) Frolov, S. V.; Kloc, C.; Schön, J. H.; Batlogg, B. *Chem. Phys. Lett.* **2001**, *334*, 65−68.
(74) Kitamura, C.; Matsumoto, C.; Kawatsuki, N.; Yoneda, A.; Kobayashi, T.; Naito, H. *Anal. Sci.* **2006**, *22*, 5−6.
(75) Robertson, J. M.; Sinclair, V. C.; Trotter, J. *Acta Crystallogr.* **1961**, *14*, 697−704.
(76) Campbell, R. B.; Robertson, J. M.; Trotter, J. *Acta Crystallogr.* **1962**, *15*, 289−290.
(77) Greyson, E. C.; Stepp, B. R.; Chen, X.; Schwerin, A. F.; Paci, I.; Smith, M. B.; Akdag, A.; Johnson, J. C.; Nozik, A. J.; Michl, J.; Ratner, M. A. *J. Phys. Chem. B* **2010**, *114*, 14223−14232.